Electrostatic Interactions of Charged Bubble Interface and Solid Wall

J. C. Hui, P. Huang
Department of Mechanical Engineering, Binghamton University, Binghamton, NY, USA

Introduction

Multiphase fluidic applications have taken root in many of today's consequential industries from energy to biology and medical diagnostics [1, 2, 3]. The U.S. Energy Information Administration estimates a rise in U.S. natural gas production from approximately 80 billion cubic feet per day in 2018 to 120 billion cubic feet per day in 2050. Natural gas is projected to continue surpassing all other fuel sources in electricity generation (estimated to produce 39% of U.S. electricity by 2050) even with the rapid growth of all renewable sources used to produce electricity (estimated to rise from 18% in 2018 to 31% by 2050) [4]. The primary process to procure natural gas in the U.S., hydraulic fracturing, has been a topic of controversy in regard to public health and environmental safety. A typical well requires about 2 to 13 million gallons of proprietary fluid (predominantly water with additives) where only 10% to 40% return to the surface as "flowback" [5]. Amid sizeable concerns for public health and environmental safety, thousands of well sites are about to be drilled in order to fulfill U.S. energy needs through the next 30 years. Incredible impact can come from innovating more efficient and safe fluidic processes for critical energy applications such as natural gas extraction.

In operations such as natural gas extraction, oversized microbubbles traveling through confined conduits have an entrained lubrication layer surrounding them [6]. As oversized microbubbles encounter obstacles and stop, those surrounding thin films can drain, leading to bubble contact with the channel walls. Such contact and adhesion create flow blockages, requiring significant increases in pressure gradient to discharge channel contents. These obstructions can be compounded due to the vast number of fissures within one natural gas well. Similarly, oversized bubble blockages can adversely affect any pumping application such as biochemical analysis or medical device design and manufacturing.

The ability to manipulate bubble shape in a flow channel would unlock new possibilities. Surface tension and hydrodynamic boundary conditions are the typical determining parameters of bubble deformation, but another method for influencing interfacial behavior is through electrostatic interactions. Surfactant molecules are widely implemented during industrial processes to stabilize emulsions as they commonly have hydrophilic heads and lipophilic tails that naturally adsorb to liquid/liquid or liquid/gas interfaces [7, 8]. If these interfacially adsorbed surfactants possess sufficient charges and an electric field exists in the domain, electrostatic forces may modify the bubble geometry. Another implementation could be through Pickering emulsions in which solid particles self assemble along liquid/liquid and liquid/gas interfaces. They can be densely packed and prevent emulsion coalescence [9]. As such, if densely packed nanoparticles held a sufficient charge, the interface would effectively hold a charge. As this charged interface encounters an external electric field, electrostatic interactions on the adsorbed particles could deform the interface. Such environments could possibly prevent lubrication layer drainage, and affect other bubble/channel or bubble/bubble interactions. Surfactants and densely packed nanoparticles would additionally modify the surface tension and hydrodynamics in ways beyond the scope of this investigation, which strictly looks at electrostatic influence on interfacial behavior.

We theorize that if electric charges are introduced at the channel wall and bubble interface, the bubble interface can be manipulated through local repulsive or attractive forces toward the channel wall. Quantifying such behavior could shed light on the potential for maintaining a thin film for oversized bubbles in a microchannel, multiple bubble interactions, or even new geometries for thermal applications. With the basic characterization of key parameters such as interfacial and wall potential, ionic concentration in the bulk, and surface tension, the understanding of electrostatic contributions to bubble morphology can be applied to the industrial fields described above.

Theory

Surface Tension

A free air bubble in water exhibits a spherical equilibrium shape. A continuous phase liquid, like water, has cohesive intermolecular forces due to hydrogen bonds [10]. As such, exposed surfaces experience a tension pulling toward the rest of the bulk where the minimal energy required results in minimal exposed surface area. Conventional surface tension units in Newtons per square meter, could be understood as the force required to maintain the surface area of a liquid interface by a unit area. Geometrically, this minimal energy state is a sphere, where the pressure difference between the surrounding bulk fluid and internal gas equals the tension force along the interface.

An oversized bubble moving along a channel deforms, exhibiting bullet-like shapes with an entrained lubrication layer surrounding it [11]. These indicate varying local pressures and shear stresses acting on the interface, inducing a bubble morphology that requires new geometries for energy balance. High velocities dramatically impact bubble shape, but lower velocity conditions cause less deformation. For stationary bubbles, symmetrical shapes are observed following the described surface tension concepts.

Transport Modeling

Incompressible, Newtonian fluid modeling conserves mass and momentum by the continuity in Eq. (1) and the Navier-Stokes equation in Eq. (2)

$$\rho \nabla \cdot \vec{u} = 0, \tag{1}$$

$$\rho \frac{\partial \vec{u}}{\partial t} + \rho(\vec{u} \cdot \nabla)\vec{u} = \nabla \cdot \left[-p\vec{I} + \mu\left(\nabla \vec{u} + (\nabla \vec{u})^T\right)\right] + \vec{F}, \tag{2}$$

where ρ is density, $\vec{u}$ is velocity vector, μ is dynamic viscosity, p is pressure, $\vec{I}$ is the identity vector, and $\vec{F}$ represents external forces. Eq. (1) and (2) can also be expanded to describe multiphase flows where more than one fluid is in the domain. One can treat the dispersed phase as a second continuous phase with another iteration of Eq. (1) and (2), where averaging of phases is needed and boundary conditions with interaction terms may be difficult. For separated flows, modeling each of the individual phases can be independently described by both equations with kinematic/dynamic boundary conditions at the interface [12].

Similarly, mass transport conserves chemical species and can be described by

$$\frac{\partial c}{\partial t} + \nabla \cdot (-D\nabla c_j) + \vec{u} \cdot \nabla c_j = R_j \tag{3}$$

for every species j, where c_j is the concentration of j, D_j is the diffusion coefficient of j, R_j is the rate of generation of j, and $\vec{u}$ is the flow velocity. Eq. (3) essentially draws from the time rate of change of concentration, species diffusion, species advection and species generation to describe the mass conservation within a differential volume [13].

Electric Double Layer

The electric potential is defined in relation to the electric field as

$$\vec{E} = -\nabla \phi, \tag{4}$$

where $\vec{E}$ is the electric field, and ϕ is the electric potential. Gauss' law describes the electric field within dielectric materials as

$$\nabla \cdot \vec{D} = \rho_e, \tag{5}$$

where $\vec{D}$ is the electric displacement field and ρ_e is the space charge density [14]. These fundamental relationships describe electric charge behavior and the electric field within dielectric media.

A charged boundary in contact with an ionic solution develops an electric double layer (EDL). In an effort to reach electrostatic equilibrium, counter-ions are drawn toward the boundary while co-ions are repelled, thus forming the EDL region that screens the electrostatic effects of the boundary charges from the bulk fluid [15]. The electrostatic strength of the charged walls is typically represented by ζ, the wall ζ-potential. Due to the Boltzmann distribution of the ions in the EDL, the near-wall electric potential follows

$$\phi(x) = \zeta e^{-x/\lambda} \tag{6}$$

if the Debye-Huckel approximation conditions are satisfied. Here, x is the distance from the charged wall and

$$\lambda = \left(\frac{F^2}{\epsilon \epsilon_0 RT} \sum_j z_j^2 C_{j,b} \right)^{-1/2} \tag{7}$$

is the Debye length that characterizes the thickness of the EDL. F is the Faraday constant, ϵ is the fluid dielectric constant, ϵ_0 is the vacuum permittivity, R is the universal gas constant, T is the fluid temperature, z_j is valence of ion j, and $C_{j,b}$ is the concentration of ion j in the fluid bulk. As shown in Eq. (6) and (7), ionic concentration is a major factor that affects the

Debye length and the overall electric potential distribution. For a given wall charge, a high concentration of ions provides more charges to screen the effect of ζ, resulting in a thinner EDL. Conversely, a lower concentration of ions cannot as readily supply charges to neutralize ζ, resulting in a thicker EDL. A thicker EDL extends the reach of wall charges farther into the fluid bulk.

Model

Geometry

In order to characterize interfacial behavior of electrostatic forces acting on a charged bubble, a model was developed to determine a possible range of repulsive and attractive interactions due to electric potential. This model placed a spherical bubble of radius, $r_0 = 50$ μm, in a cylindrical water filled microchannel of radius, $r_c = 50.2$ μm, as shown in Fig. 1. The 200 nm initial spacing between the bubble interface and channel wall would be sufficient for a near overlap of Debye lengths if the bulk symmetric electrolyte concentrations, C_1 and C_2 (collectively referred to as $C_{j,b}$), are on the order of 10 μM. Additionally, the outlet at the top was placed sufficiently far away from the bubble to avoid inlet or outlet interference to the flow. A surface ζ-potential on the channel wall would provide an electrostatic environment for the charged interface to interact with, and after the bubble reaches an equilibrium position, the final interfacial displacement, d_f , away from r_0 at the horizontal symmetry plane, $z = 0$, could be measured for each parametric case.

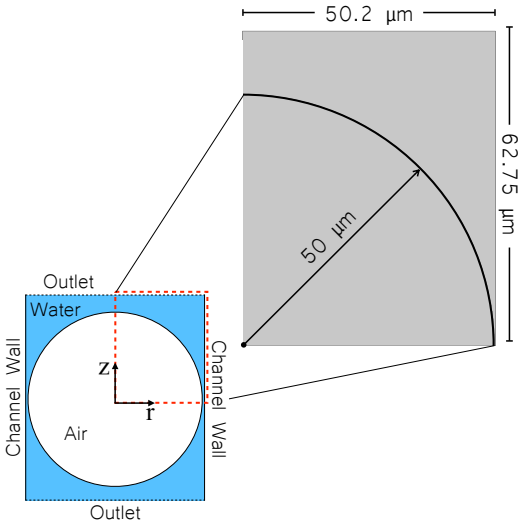

Figure 1. 2D axisymmetric view of spherical air bubble geometry in water-filled microchannel

Boundary Conditions

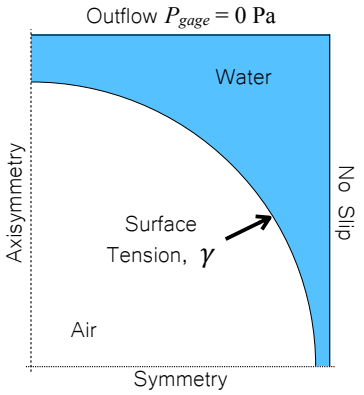

(a) Fluid Mechanics

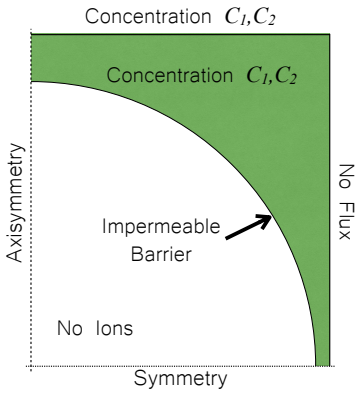

(b) Transport of Dilute Species

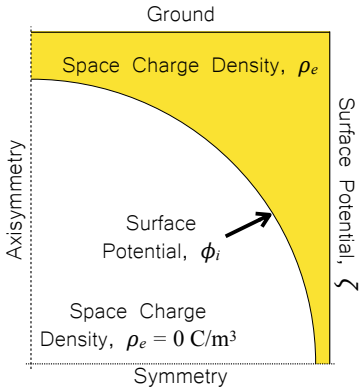

(c) Electrostatics

Figure 2. Boundary conditions of governing equations, viewed in 2D axisymmetry with horizontal planar symmetry

This multiphysics model incorporates 3 sets of coupled governing equations and boundary conditions to handle all of the parameters in action. Namely, numerical solutions to the conservation of mass and momentum for fluid mechanics, species conservation

for mass transport, and Maxwell's equations for electrostatics are sought simultaneously. With axisymmetry and planar symmetry of the cylindrical channel and spherical bubble, we define the boundary conditions for each physical aspect as shown in Fig. 2. Here, we model one quarter of a channel cross-section where the left boundary is the channel axis. The channel wall and the channel outlet are at the right and top boundaries, respectively. The bubble, which has a defined surface tension γ, holds zero axial velocity as there is no pressure gradient along the channel. A symmetric electrolyte concentration of $C_{j,b}$ composed of positive and negative ions, C_1 and C_2, is defined at the outlet boundary and in the water bulk. The interface between the air and water is treated as an impermeable barrier to ions. The channel wall and bubble interface have surface potentials ζ and ϕ_i, respectively. The ionic water is capable of holding a space charge density, ρ_e, corresponding to local ionic concentrations influenced by the surface potentials.

Module Setup

In order to develop a COMSOL model for this multiphase multiphysics problem, three modules are fully coupled with a customized weak contribution. In order to capture the interfacial movement with a high resolution, COMSOL's Two Phase Flow Moving Mesh Module (TPFMM) was selected to accurately mark the exact position of the interface as the interface deforms. The Electrostatics Module (ES) is used to apply an electric potential on the channel wall and bubble interface, ground the channel outlet, and calculate the electric field across the domain. The Transport of Dilute Species Module (TDS) utilizes the mass conservation equations to model ionic transport throughout the domain. In order for capture all physical interactions appropriately, all of the governing equations from each module must be fully coupled. Fig. 3 describes how the the three modules are linked by variables. ES takes $C_{j,b}$ from TDS to compute ρ_e and $\vec{E}$. TPFMM uses $\vec{E}$ from ES to calculate interfacial movement and liquid flow. TDS takes V from ES and $\vec{u}$ from TPFMM to determine the ion distribution in the water. Built-in COMSOL options easily couple all these modules except ES and TPFMM via $\vec{E}$, shown with the red arrow. No default coupling option of electrostatic forces for interfacial deformation exists, so a customized weak contribution was developed to link TPFMM and ES. As a transient model, this setup solves the stationary case first to establish the EDL, and then solves the transient bubble deformation until an equilibrium shape was reached. By solving for the stationary EDL first, computation time is saved as the time scale of establishing the EDL is much shorter than the interfacial deformation time scale, and the process of EDL establishment does not impact the final bubble equilibrium shape.

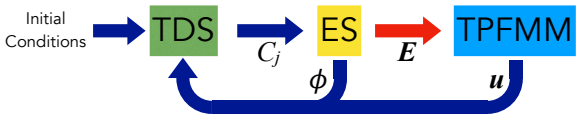

Figure 3. Variable coupling among COMSOL modules

Developing the Weak Formulation

Consider a laminar, viscous flow of a gas bubble deforming in a restrictive cylindrical flow channel filled with a liquid and exposed to an electric field. If gravitational force is negligible, the Navier-Stokes equation takes the form of

$$\rho\left[\frac{\partial\vec{u}}{\partial t}+(\vec{u}\cdot\nabla)\,\vec{u}\right]=\nabla\cdot\bar{\bar{\sigma}} \tag{8}$$

where $\bar{\bar{\sigma}}$ is the total stress tensor. The boundary condition at a two-fluid interface takes the form of

$$\hat{n}\cdot(\bar{\bar{\sigma}}_A-\bar{\bar{\sigma}}_B)=\Gamma\gamma\hat{n}-\nabla_s\gamma-\rho_s\nabla\phi \tag{9}$$

where $\hat{n}$ is the outward unit normal vector pointing from fluid B (gas) to fluid A (liquid), $\Gamma\equiv\nabla_s\cdot\hat{n}$ is the local interface curvature,

$$\nabla_s=\left(\bar{\bar{I}}-\hat{n}\hat{n}\right)\cdot\nabla=\nabla-\hat{n}\frac{\partial}{\partial n} \tag{10}$$

is the gradient operator in the boundary surface curvilinear coordinate, γ is surface tension between the two fluids, ρ_s is the interface surface charge density, and ϕ is the electric potential experienced by the interfacial charges.

In finite element analysis, the governing equation and interfacial boundary conditions are applied through the weak formulation [16]. First, Eq. (8) is multiplied with a test vector function $\vec{v}$, and then integrated over the volume of the fluid of interest Ω,

$$\int_\Omega\rho\left[\frac{\partial\vec{u}}{\partial t}+(\vec{u}\cdot\nabla)\,\vec{u}\right]\cdot\vec{v}\,d\Omega=\int_\Omega(\nabla\cdot\bar{\bar{\sigma}})\cdot\vec{v}\,d\Omega. \tag{11}$$

Integrating the divergence of the total stress term by parts leads to

$$\int_\Omega\rho\left[\frac{\partial\vec{u}}{\partial t}+(\vec{u}\cdot\nabla)\,\vec{u}\right]\cdot\vec{v}\,d\Omega= -\int_\Omega\nabla\vec{v}:\bar{\bar{\sigma}}\,d\Omega+\int_S\vec{v}\cdot(\hat{n}\cdot\bar{\bar{\sigma}})\,dS \tag{12}$$

where S represents the surface bounding Ω. The surface integral is evaluated based on the imposed boundary conditions and is handled as boundary weak contribution in COMSOL. Suppose fluid B is a gas such that $\bar{\bar{\sigma}}_B \approx 0$ and $\bar{\bar{\sigma}}_A = \bar{\bar{\sigma}}$. Applying Eq. (9) to the surface integral in Eq. (12), we get

$$\int_S \vec{v} \cdot (\bar{\bar{\sigma}} \cdot \hat{n})\, dS = \int_S \vec{v} \cdot [(\nabla_s \cdot \hat{n})\, \gamma \hat{n}]\ dS - \int_S \vec{v} \cdot \nabla_s \gamma dS - \int_S \vec{v} \cdot \rho_s \nabla \phi\, dS, \quad (13)$$

where we have used $\Gamma = \nabla_s \cdot \hat{n}$. To proceed further, we make use of the surface divergence theorem [17] where for any arbitrary vector $\vec{w}$,

$$\int_S (\nabla_s \cdot \hat{n})\, (\vec{w} \cdot \hat{n})\ dS = \int_S \nabla_s \cdot \vec{w}\, dS - \int_C \vec{w} \cdot \hat{m} dC \quad (14)$$

where C is the contour that bounds surface S and $\hat{m}$ is a unit vector that is simultaneously normal to C and $\hat{n}$. Rewriting Eq. (13) by applying the surface divergence theorem of Eq. (14), we get

$$\int_S \vec{v} \cdot (\bar{\bar{\sigma}} \cdot \hat{n})\, dS = \int_S \gamma\, (\nabla_s \cdot \vec{v})\ dS - \int_S \vec{v} \cdot \rho_s \nabla \phi\, dS - \int_C \gamma \vec{v} \cdot \hat{m}\, dC, \quad (15)$$

where we have applied the vector calculus identity of

$$\nabla_s \cdot (\gamma \vec{v}) = \vec{v} \cdot \nabla_s \gamma + \gamma\, (\nabla_s \cdot \vec{v})\,. \quad (16)$$

Substituting Eq. (15) into Eq. (12) we get

$$\int_\Omega \rho \left[\frac{\partial \vec{u}}{\partial t} + (\vec{u} \cdot \nabla)\, \vec{u} \right] \cdot \vec{v}\, d\Omega = - \int_\Omega \nabla \vec{v} \colon \bar{\bar{\sigma}}\, d\Omega + \int_S \gamma\, (\nabla_s \cdot \vec{v})\ dS - \int_S \vec{v} \cdot \rho_s \nabla \phi\, dS - \int_C \gamma \vec{v} \cdot \hat{m}\, dC, \quad (17)$$

which is the complete weak form governing equation of interfacial deformation between a liquid and a gas due to surface tension and electrostatic force.

Finally, the contour integral in Eq. (17) must be considered only if there exists a contact line and is critical in modeling contact line dynamics. That is, the contour integral term is non-zero only if the gas bubble makes contact with the channel wall. In our model, we focus on the bubble interface deformation before it makes contact with the channel wall. Therefore without any contact line, the contour integral term is zero in our model. This reduces Eq. (17) to

$$\int_\Omega \rho \left[\frac{\partial \vec{u}}{\partial t} + (\vec{u} \cdot \nabla)\, \vec{u} \right] \cdot \vec{v}\, d\Omega = - \int_\Omega \nabla \vec{v} \colon \bar{\bar{\sigma}}\, d\Omega + \int_S \gamma\, (\nabla_s \cdot \vec{v})\ dS - \int_S \vec{v} \cdot \rho_s \nabla \phi\, dS. \quad (18)$$

We also note that in this weak formulation the variable to be solved in Eq. (18) is $\vec{u}$ while ϕ is considered as given. Thus a test function for ϕ is not needed to reduce its order of differentiation.

Implementing the Weak Contribution

The electrostatic force acting on the bubble surface is captured by the last term of Eq. (18). This must be implemented as weak contribution in appropriate COMSOL syntax. In COMSOL, basis functions (test functions) are established through test operators. Here, we are interested in solving for velocity, which in cylindrical coordinates has components in the $\hat{r}$, $\hat{\theta}$, and $\hat{z}$ directions. The test operators must operate on the velocity components corresponding to the direction in which the basis functions are trying to approximate.

To implement the electrostatic boundary conditions, an electric potential is defined on the bubble surface. As such, the gradient of electric potential, $\nabla\phi$, and the surface charge density, ρ_s, need to be represented by the electric field. Electromagnetic theories indicate

$$\vec{E} = -\nabla \phi, \quad (19)$$

and

$$\rho_s = \varepsilon \varepsilon_0 \left(\vec{E} \cdot \hat{n} \right), \quad (20)$$

where ε is the dielectric constant of water and $\hat{n}$ is the normal unit vector on the bubble surface toward the water. Substituting Eq. (19) and Eq. (20) into the last term of Eq. (18), we have

$$- \int_S \vec{v} \cdot \rho_s \nabla \phi\, dS = \int_S \vec{v} \cdot \varepsilon \varepsilon_0 \left(\vec{E} \cdot \hat{n} \right) \cdot (\vec{E})\, dS. \quad (21)$$

With 2D axisymmetry, Eq. (20) becomes

$$\rho_s = \varepsilon \varepsilon_0\, (E_r n_r \hat{r} + E_z n_z \hat{z}) \quad (22)$$

and Eq. (21) can be written as

$$- \int_S \vec{v} \cdot \rho_s \nabla \phi\, dS = \int_S v_i \varepsilon \varepsilon_0\, (E_r n_r \hat{r} + E_z n_z \hat{z})\, (E_r \hat{r} + E_z \hat{z})\, dS. \quad (23)$$

Converting to COMSOL syntax, the right-hand side of Eq. (23) can be written as

"`mat1.epsilonr*epsilon0_const* [es.Er*nr+es.Ez*nz]*[test(u)*es.Er+ test(w)*es.Ez]`"

which is inserted as the weak contribution term on the right hand side of the Navier-Stokes equation in a 2D axisymmetric TPFMM case, completing the coupling of the electric field with interfacial deformation.

Results

The main objective of this investigation was to understand how electrostatic interactions in this multiphysics environment may affect bubble surface repulsion or attraction to the channel wall. The key parameter used to quantify repulsive or attractive behavior between the bubble surface and the charged channel wall is d_f. A baseline bubble with no electrostatic interactions was found to maintain a spherical shape where $d_f = 0$ nm, equivalent to no deformation. The equilibrium state of charged cases showed that the bubble radius at $z = 0$ is consistently the nearest interfacial point to the wall, suggesting d_f as a strong metric of the electrostatic force effects on the interface. $C_{j,b}$ and ϕ_i are observed to be important parameters affecting d_f. Each parametric combination demonstrated varying degrees of repulsion and attraction as shown in Fig. 4. On this plot, d_f vs. $C_{j,b}$ between 10 μM and 600 μM under six different values of ϕ_i is shown. For all data, ζ is fixed at 50 mV.

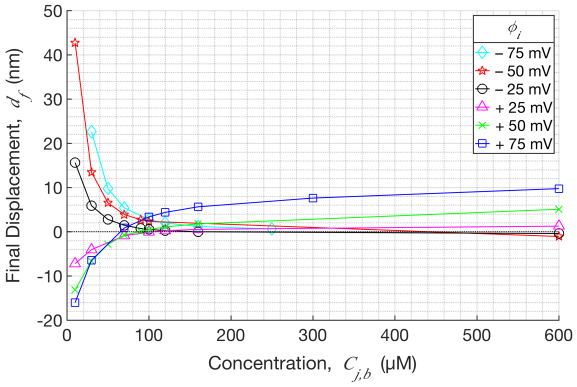

Figure 4. d_f for varying $C_{j,b}$ and ϕ_i at ζ = 50 mV

Repulsive behavior is observed for cases of positive ϕ_i at low $C_{j,b}$. At one extreme, $C_{j,b}$ = 10 μM and ϕ_i = 75 mV produces a repulsive displacement of d_f of -16 nm. Fig. 5a illustrates the EDL across the thin film at equilibrium with the initial thin film starting at the black line at r_0. Less repulsive displacement is observed as $C_{j,b}$ increases. The trend from positive ϕ_i cases indicate that for + 25 < ϕ_i < +75 mV repulsion can be achieved at $C_{j,b}$ < 70 μM. This can be explained by the Boltzmann distribution of ions in the EDL, where at lower ionic concentrations the EDL screening effect is weaker. This effectively enables the charged wall and bubble surface to have an electrostatic reach farther into the water bulk. Additionally, as the concentration increases above 70 μM in the 50 mV and 75 mV cases, a surprisingly flipped behavior arises where the d_f reveals a weak attraction. This could be due to an added effect of highly concentrated ions in the EDL near the bubble surface and the wall. Nevertheless, repulsive behavior is clearly observed under low ionic concentration with high bubble surface and wall electric potentials.

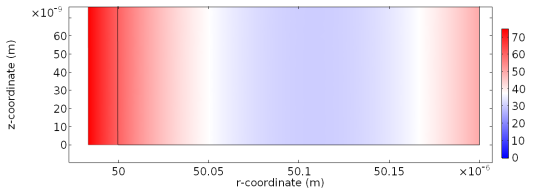

(a) $\phi_i = 75$ mV

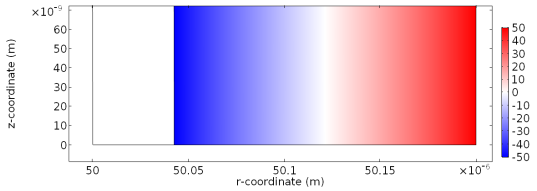

(b) $\phi_i = -50$ mV

Figure 5. ϕ across thin film at equilibrium when $C_{j,b} = 10$ μm and ζ = 50 mV

Attractive behavior is seen for all of the negative ϕ_i and sufficiently low $C_{j,b}$ cases. The greatest attractive d_f observed is 42.7 nm at $\phi_i = -50$ mV and $C_{j,b} = 10$ μM. Fig. 5b shows the symmetrical EDL profile across the thin film with the initial interface location at the black line at r_0. All negative ϕ_i cases seem to exhibit little to no variation from the baseline ($d_f = 0$ nm) at sufficiently high $C_{j,b}$ (above 100-200 μM), which affirms that the electric potentials of the bubble surface and the channel wall are well screened by the EDL (λ < 30 nm on both sides of gap). Attraction appears to increase with increasingly negative ϕ_i and decreasing $C_{j,b}$. This intuitively agrees with how lower $C_{j,b}$ increases the range of an electric potential's influence with less available screening ions, while higher $C_{j,b}$ provide sufficient

ions in the EDL to screen out the electric field created by the opposite charges of the bubble surface and the channel wall.

Conclusions

In summary, we created a COMSOL multiphysics model to quantify repulsive and attractive interactions between a charged bubble surface and a charge channel wall. A custom weak contribution was derived and implemented in COMSOL to appropriately couple interfacial electric force and bubble surface deformation. The simulation results show that the combination of electric potential and ion concentration for a given geometry are important factors that dictate interfacial deformation. With larger electric potentials of like polarity, thicker thin films can be maintained, but only below a certain threshold of ion concentration. The data gathered prescribes the ability to develop repulsive electrostatic environments and points to the possibility of precluding bubble contact in confining conduits where greater electric potentials, different bubble geometries, and varying material properties could facilitate repulsive behavior. In our future research, we will use the developed COMSOL model to strategically study oversized bubbles and electric parameters to better understand the interfacial repulsion and attraction.

References

[1] D. E. Angelescu, B. Mercier, D. Siess, and R. Schroeder. Microfluidic capillary separation and real-time spectroscopic analysis of specific components from multiphase mixtures. *Analytical Chemistry*, 82:2412–2420, 2010.

[2] E. K. Sackmann, A. L. Fulton, and D. J. Beebe. The present and future role of microfluidics in biomedcial research. *Nature*, 507:181–189, 2014.

[3] M. A. McClain, C. T. Culbertson, S. C. Jacobson, N. L. Allbritton, C. E. Sims, and J. M. Ramsey. Microfluidic devices for the high-throughput chemical analysis of cells. *Analytical Chemistry*, 75:5646–5655, 2003.

[4] Annual Energy Outlook 2019 with projections to 2050. Technical report, U.S. Energy Information Administration, Washington, DC, 2019.

[5] A. Vengosh, R. B. Jackson, N. Warner, T. H. Darrah, and A. Kondash. A critical review of the risks to water resources from unconventional shale gas development and hydraulic fracturing in the united states. *Environ. Sci. Technol.*, 48:8334–8348, 2014.

[6] M. K. Mulligan and J. P. Rothstein. Deformation and Breakup of Micro- and Nanoparticle Stabilized Droplets in Microfluidics Extensional Flows. *Langmuir*, 27(16):9760–9768, July 2011.

[7] Y. K. Takahara, S. Ikeda, S. Ishino, K. Tachi, K. Ikeue, T. Sakata, T. Hasegawa, H. Mori, M. Matsumura, and B. Ohtani. Asymmetry modified silica particles: A simple particulate surfactant for stabilization of oil droplets in water. *J. Am. Chem. Soc.*, 127:6271–6275, 2005.

[8] P. J. Wilde. Interfaces: their role in foam and emulsion behavior. *Current Opinion in Colloid & Interface Science*, 5:176–181, 2000.

[9] T. N. Hunter, R. J. Pugh, G. V. Franks, and G. J. Jameson. The role of particles in stabilising foams and emulsions. *Advances in Colloid and Interface Science*, 137:57–81, 2008.

[10] J. N. Israelachvili. *Intermolecular and surface forces*. Academic press, 2015.

[11] V. S. Ajaev and G. M. Homsy. Modeling shapes and dynamics of confined bubbles. *Ann. Rev. Fluid Mech.*, 38:277–307, 2006.

[12] J. D. Schwarzkopf, M. Sommerfeld, C. T. Crowe, and Y. Tsuji. *Multiphase flows with droplets and particles*. CRC press, 2011.

[13] William M Deen. *Analysis of transport phenomena*, volume 2. Oxford University Press New York, 1998.

[14] COMSOL AB, Stockholm, Sweden. *COMSOL Multiphysics Reference Manual*, 5.2a edition, 2016.

[15] R. J. Hunter. *Zeta potential in colloidal science*. Academic Press Inc., San Diego, CA, 1981.

[16] Xiaodong Chen, Rachel Zielinski, and Samir N. Ghadiali. Computational Analysis of Microbubble Flows in Bifurcating Airways: Role of Gravity, Inertia, and Surface Tension. *Journal of Biomechanical Engineering*, 136(10):101007, Aug 2014.

[17] M. A. Walkley, P. H. Gaskell, P. K. Jimack, M. A. Kelmanson, and J. L. Summers. Finite Element Simulation of Three-Dimensional Free-Surface Flow Problems. *Journal of Scientific Computing*, 24(2):147–162, Aug 2005.

Acknowledgements

The authors would like to recognize and thank the American Chemical Society under grant ACS PRF 53371-ND9 for supporting this work.